LAWRENCE
LIVERMORE
NATIONAL
LABORATORY

LLNL-JRNL-828696

Counter-ion effect on the diffusion behavior of Yb, Lu, and Nd ions in YAG transparent ceramics

T. J. Rudzik, Z. M. Seeley, F. Ryerson, N. J. Cherepy, S. A. Payne

November 2, 2021

Optical Materials: X

Disclaimer

Counter-ion effect on the diffusion behavior of Yb, Lu, and Nd ions in YAG transparent ceramics

Thomas J. Rudzik[a*], Zachary M. Seeley[a], Frederick J. Ryerson[a], Nerine J. Cherepy[a], and Stephen A. Payne[a]

[a] Lawrence Livermore National Laboratory, 7000 East Avenue, Livermore, CA, 94550

Abstract

The ability to fabricate additively manufactured laser waveguides with sharp dopant concentration interfaces is limited by diffusion of the dopants at the temperatures required to fully densify the material. Compositional analysis of bilayer samples, where each layer was either undoped YAG or YAG doped with Yb, Lu, or Nd, were fabricated such that all combinations were available for testing. Samples were fabricated at both 1750°C and 1850°C to determine the diffusion behavior of each dopant alone and also in the presence of a second dopant. It was found that the experimental concentration profiles exhibited both intragranular (bulk) and grain boundary contributions, and thus fitting to a complementary error function equation required the use of two diffusion coefficients. Nd always diffused further along grain boundaries than the other dopants, due in part to its small segregation coefficient in YAG. It is shown that the presence of Nd as a counter dopant inhibits intragranular diffusion of other dopants while enhancing their grain boundary diffusion. All the observed trends were attributed to a combination of intragranular lattice strain due to: dopant ions replacing yttrium substitutionally, the relative driving forces for the segregation of dopant ions to grain boundaries, and the ability of one dopant to affect the diffusion of a different dopant in the other direction to maintain charge neutrality.

Keywords

Transparent ceramic; Intragranular and intergranular diffusion; YAG; Counterion; Concentration profile fitting; Nd, Yb, Lu

1. Introduction

In the field of laser design, there is a demand for more complex gain media offering capabilities unachievable with conventional single crystals. Transparent optical ceramic gain media provide opportunities to avoid or mitigate some of the limitations of single crystals and have been broadly researched over the past few decades [1,2,3]. Some advantages include: large sizes, lower-cost growth, improved mechanical toughness, forming optically contiguous composites, and incorporating graded or distinct regions of different doping concentrations [4-15], which can be achieved by fabrication techniques such as additive manufacturing [16]. Two examples of additively manufactured Yttrium Aluminum Garnet (YAG) ceramic laser gain media are core-clad Nd-doped rods [4, 11] and planar waveguides with a thin Yb-doped central region [8-10,15]. To achieve a uniform refractive index in these optics, non-spectroscopic dopants (e.g., Lu) were required in the non-active regions of these YAG ceramics, but even so, differential diffusion of Nd, Yb, Lu and any other dopants in YAG must be carefully managed [4, 8-11,13,15]. It has become clear that maintaining the as-deposited doping geometry is limited by ionic diffusion inherent to the elevated sintering temperatures required to densify the doped powders into transparent ceramics.

The general phenomenon of counter-ion effects in diffusion is well-known in metals as the Kirkendall Effect [17]. Previous studies in ceramics have reported differences between the diffusion coefficients for Nd and Yb dopants crossing an interface from Lutetium Aluminum Garnet (LuAG) into YAG, both individually and concurrently [7], as well as Yb diffusion and Nd diffusion in Yb:YAG/YAG composites [6], and Nd:YAG/YAG composites, respectively [5]. However, research focused on diffusion of Nd, Yb, and Lu dopants moving in opposing directions in YAG has not been reported. Here we report on our investigations into how the linear diffusion of rare earth (RE) dopants is affected by the presence of other rare earth dopants diffusing in the opposite direction simultaneously. Additionally, the effect of the maximum processing temperature on the diffusion distance of different dopants was studied.

2. Experimental Procedure

Starting powders of YAG, 10%Yb:YAG, 16%Lu:YAG, and 3%Nd:YAG were supplied by Nanocerox (Ann Arbor, MI). Aqueous powder-loaded slurries with 0.5 wt% TEOS, 300 MW PEG, and Darvan were spray dried. The spray dried powders were loaded sequentially into a die to form layers with different dopants. Samples were cold pressed, subjected to 30 ksi in a cold isostatic press, burned out at 1000°C in air, vacuum sintered at 1550°C, and made transparent via hot isostatic pressing using 29 ksi and either 1750°C or 1850°C with a dwell time of 4 hours. The resulting samples, as shown in Figure 1, had no residual porosity or secondary phases present and were thus transparent.

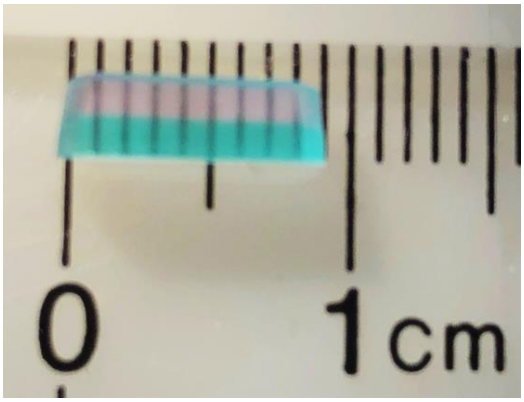

Figure 1. Photograph of a 10% Yb:YAG|3%Nd:YAG sintered and polished 2.57 mm thick sample, laying on grid paper. This sample is comprised of two regions with different dopants, Yb (blue-green, due to residual Yb^{2+} absorption) on the bottom and Nd (purple, due to Nd^{3+} absorption) on the top, with a distinct linear interface between them. Despite the presence of the Yb^{2+} color, over 99% of the total Yb ions are in the 3+ oxidation state.

Compositional microanalyses were collected on a JEOL-8530 electron microprobe operating at 20 kV with a 200 nA focused electron beam. On-peak X-ray intensities were measured for the Al Kα, Y Lα Nd Lα, Yb Lα and Lu Lα lines with peak count times of 20 s. Background intensities were determined using a mean atomic number (MAN) calibration method utilizing an array of standard materials [18]. When practical, the x-ray intensity for each lanthanide was collected on multiple spectrometers equipped with LiF analyzing crystals. X-ray intensities were converted to oxide compositions using the CITZAF correction scheme [19] with YAG, Nd-Ga garnet and lanthanide-bearing glasses as primary standards. Experimental lineouts of dopant profiles were fit and analyzed using Origin Pro®[20].

3. Results and Discussion

3.1 Diffusion in the bulk and along grain boundaries:

The elevated temperatures required for consolidation of the bi-layer ceramics resulted in diffusion of the rare earth ions across the boundary between the two layers deposited in the die. Rare earth ion concentrations were measured in each sample along lines perpendicular to the interface via electron probe measurements at 1 μm intervals on well-polished cross-sections of each sample. The resulting data was fitted to determine the diffusion constants via the commonly used one-dimensional solution to Fick's Second Law [5]:

$$C = \frac{C_0}{2} erfc\left(\frac{x-\mu}{2\sqrt{Dt}}\right) \quad (1)$$

where C is the concentration of the diffusing species with respect to distance, x, from the interface, μ, at time t, C_0 is the initial concentration of the dopant at time t=0 for positions x<μ, D is the diffusion coefficient, and erfc is the complementary error function.

For the concentration line scan of each rare earth (RE) species, the parameters in the equation were modified until a good fit to the experimental data, in terms of percentage of RE sites occupied vs distance along the line scan, was achieved (see Figure 2). The percentage of rare earth sites occupied was calculated as:

$$\%RE_A = \left(\frac{at\%A}{at\%Y + at\%A + at\%B}\right) \times 100\% \quad (2)$$

where $\%RE_A$ is the percentage of RE sites occupied by dopant species A, and at% A, at% B, and at% Y are the atomic percent of dopant A, the counter dopant B, if present, and Yttrium, respectively. The diffusion coefficient in the fit was then taken to be the diffusion coefficient of the corresponding data. It was found that a good fit to the 1750°C sample data could be produced using only Equation 1, but later for 1850°C samples it was determined that an accurate fit required a combination of two such expressions, each with a different diffusion coefficient. Upon reaching this conclusion, the 1750°C fits were made to a 2-coefficient expression as well. In this work, the presence of different diffusion processes was modeled using the equation:

$$C = F\left(\left(\frac{\Delta C}{2}\right) erfc\left(\frac{x-\mu}{2\sqrt{D_1 t}}\right)\right) + (1-F)\left(\left(\frac{\Delta C}{2}\right) erfc\left(\frac{x-\mu}{2\sqrt{D_2 t}}\right)\right) \quad (3)$$

where ΔC is the dopant concentration range, used in place of C_0 to enable fitting of data that does not go to zero concentration (yttrium), D_1 and D_2 are diffusion coefficients corresponding to independent diffusion processes and F is the fraction representing the relative contribution of each process to the experimental results. The need to account for multiple contributions to diffusion in polycrystalline ceramics has been reported previously [6,21,22], and the separate expressions for diffusion were assigned to diffusion within grains (bulk or intragranular diffusion) and diffusion along grain boundaries. Employing this explanation for the samples described here, the smaller diffusion constant is assigned to the bulk contribution and the larger diffusion constant to the grain boundary contribution.

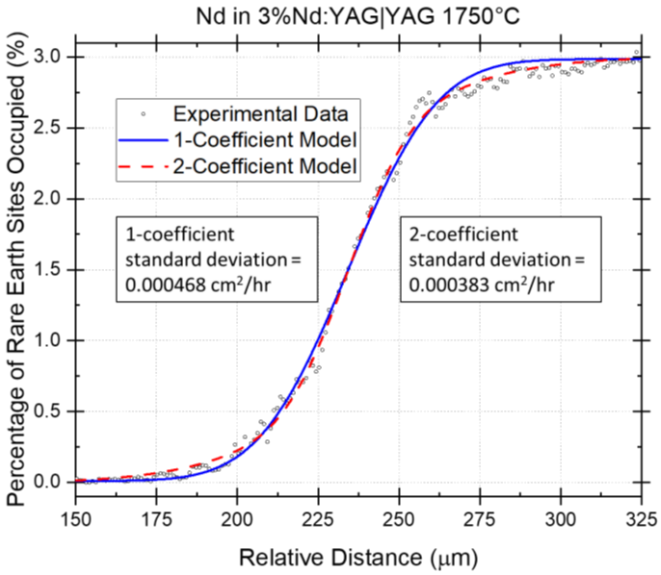

Figure 2. Nd concentration profile in the 3% Nd:YAG|YAG sample processed at 1750°C, as measured via electron probe. For the 1-coefficient model, D = 5.93×10^{-7} $cm^2/_{hr}$, and for the 2-coefficient model, F = 0.629, D_1 = 2.79×10^{-7} $cm^2/_{hr}$, D_2 = 1.85×10^{-6} $cm^2/_{hr}$. Although the difference between the fit qualities is small for this sample, the 2-coefficient model will later be shown to be far superior to the 1-coefficient model for samples processed at 1850°C and containing Nd.

The fractions corresponding to the two coefficients manifest physically as the fraction of dopant ions in each of the two regions, (i.e. "bulk" and "grain boundary" diffusion). An illustration is shown in Figure 3 (left) to visualize this concept, while the diagram (right) demonstrates movement of a dopant ion through a microstructure over time, passing through both grains and grain boundaries.

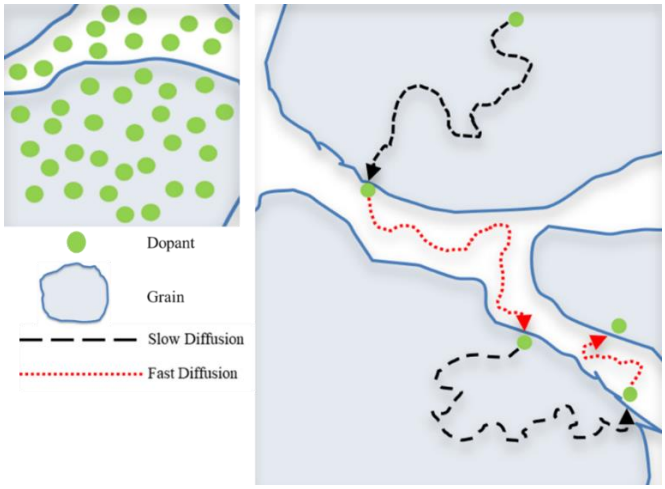

Figure 3. Illustration of a microstructure (left) with dopant ions both inside grains and at grain boundaries, which may be modeled with a two-term equation, as in Equation 3, where F manifests as the fraction of all dopant ions located in the bulk. The other image (right) shows movement of a dopant ion over time, which may include moving within grains and along grain boundaries, as well as exiting and entering grains at the boundaries.

3.2 Diffusion at 1850°C:

Samples subjected to the higher HIP temperature of 1850°C showed frequent, sharp fluctuations in RE concentrations along the scan line, as can be seen in Figure 4(a). Concentration mapping of these samples (Figure 4(b)) indicated a substantial discrepancy between concentrations in the bulk and at the grain boundaries, especially near the doping interface. This carried over to the line scan results, causing the fluctuations when crossing between the bulk and the grain boundaries (Figure 4(c)) and thus are phenomenologically the result of discrete bulk concentrations that differ from concentrations at the adjacent grain boundary .

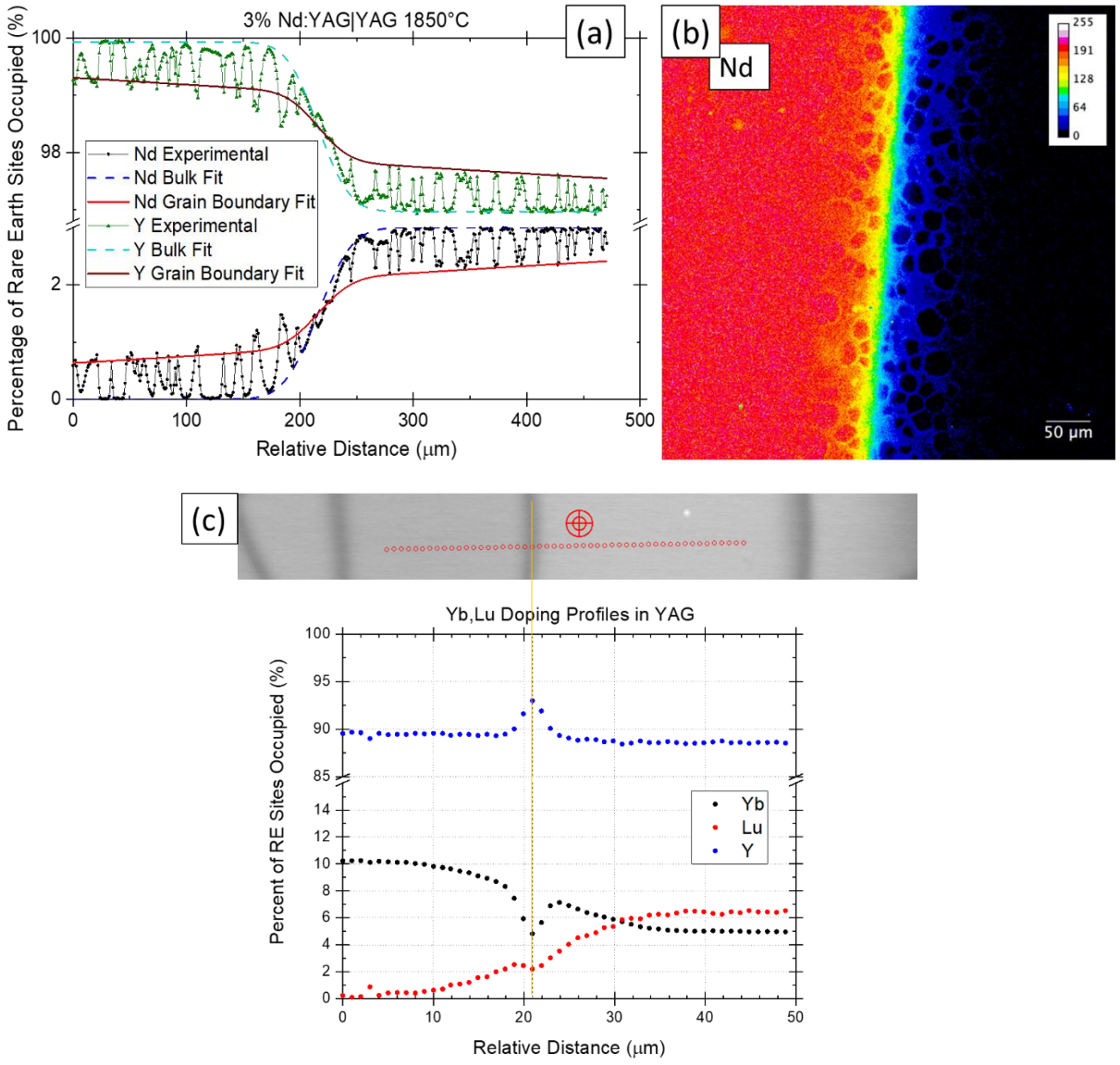

Figure 4. (a) Concentrations of rare earth species in a 3% Nd:YAG|YAG sample after processing at 1850°C. Lines between adjacent experimental data points are added to help visualize the transitions in behavior. For the Nd data, the bulk fit diffusion coefficient was $7 \times 10^{-7}\ cm^2/_{hr}$ and the grain boundary parameters were F=0.4, D_1=$7 \times 10^{-7}\ cm^2/_{hr}$, and D_2=$4 \times 10^{-4}\ cm^2/_{hr}$. The diffusion coefficient for the Y bulk fit was D=$6 \times 10^{-7}\ cm^2/_{hr}$ and the fitting parameters for the grain boundary fit were F=0.4, D_1=$6 \times 10^{-7}\ cm^2/_{hr}$, and D_2=$4 \times 10^{-4}\ cm^2/_{hr}$.

Bulk fits are shown with dashed lines and grain boundary fits are shown with solid lines. **(b)** Nd concentration map showing contrast between grains and adjacent grain boundaries near the composition interface. **(c)** A high-magnification micrograph of the 10% Yb:YAG|16%Lu:YAG 1850°C sample over which a concentration line scan was conducted, with data points shown as red circles, and a corresponding concentration plot showing the effect of crossing a grain boundary on the experimental data, thus explaining the fluctuations in **(a)**.

It is presumed that the lack of these jagged features in the data for samples processed at 1750°C (Figure 2) is attributable to the smaller grain size, as evident when comparing Figure 5(a) and Figure 5(b) as a typical example, for which the measurement equipment cannot resolve separate bulk and grain boundary concentrations and thus outputs an average of the two. Since the bulk and grain boundary concentrations could be distinguished for the 1850°C samples, the two diffusion regions were fit separately for each rare earth species, as demonstrated in Figure 4(a). It was clear from concentration maps, such as in Figure 4(b), that the RE species diffused further from the composition interface in the grain boundaries than within the grains, therefore the curves showing less diffusion (dashed lines in Figure 4(a)) must correspond to bulk diffusion. As can also be identified in this map, similarly evident in all concentration maps, only a narrow region near the interface shows noticeable loss in dopant concentration within grains on the doped side, as well as uptake of the dopant into grains on the undoped side, thereby indicating a significant contribution of bulk diffusion to the experimental composition profile localized to the immediate region around the composition interface. In the fitting of the data for all samples, the bulk diffusion data could be fit well with the single-expression Equation 1, as was expected since it is now isolated from the other diffusion process' signal.

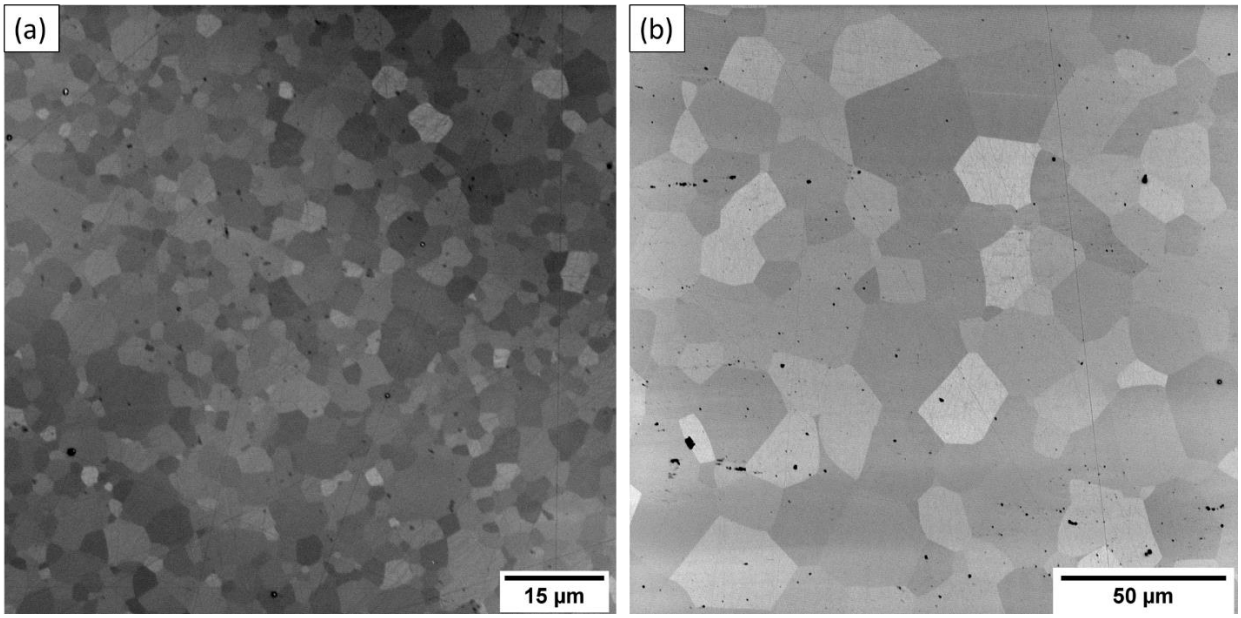

Figure 5. SEM backscatter electron micrographs of 10% Yb:YAG samples fabricated at (a) 1750°C and (b) 1850°C, showing the clear difference in average grain size resulting from the difference in fabrication temperature.

As mentioned in Section 3.1, the larger diffusion coefficient curves (solid curves in Figure 4(a)), however, required the two-expression Equation 3 to achieve a good fit. These curves, which exhibit much further displacement of the RE ions, must correspond to grain boundary diffusion since the dopant species diffused further from the composition interface at the grain boundaries than within the grains. This

suggested the coexistence of multiple processes contributing to the grain boundary diffusion. Looking at this curve, it is clear that there are two distinct regimes: one close to the composition interface with a faster change in concentration with distance and one further from the interface on either side with a more gradual but non-zero concentration change with distance. It is logical to conclude that diffusion in the near-interface regime is primarily driven by the dopant concentration difference between the two composition regions according to Fick's first law. Therefore, the expression with the smaller diffusion coefficient in Equation 3 represents the bulk grain contribution of the concentration gradient across the interface. Although the effect of bulk diffusion has already been isolated as the dashed curves in Figure 4(a), the location of the central regime in the grain boundary curves match very well with the region over which the bulk diffusion curves assert influence, as evidenced by the change in slope of both curves in the same locations. Additionally, in all fits, the diffusion coefficient which fit the bulk diffusion curve was identical to that of the smaller diffusion coefficient term of the grain boundary curve. The relationship between the two, then, is that the dopant moves between grain interiors and surfaces according to the bulk diffusion curve and from the surface of grains on the doped side to the surface of grains on the undoped side according to the central region of the grain boundary curve. Outside of the central regime, the influence of the composition interface diminishes and that of rapid movement of dopant ions along grain boundaries dominates. As such, the corresponding grain boundary diffusion coefficients are orders of magnitude larger.

3.3 Diffusion with counter-diffusing dopants

Figure 6 is an illustration of the numerous data we have acquired for two counter-diffusing ions at 1850^{o}C, in this case for the Yb dopant of a 10%Yb:YAG|16%Lu:YAG sample. In Figure 7(a,b) below, we omit the actual experimental data for clarity in that the illustrative fits in Figures (2), (4) and (6) adequately represent the fitting quality we routinely achieved.

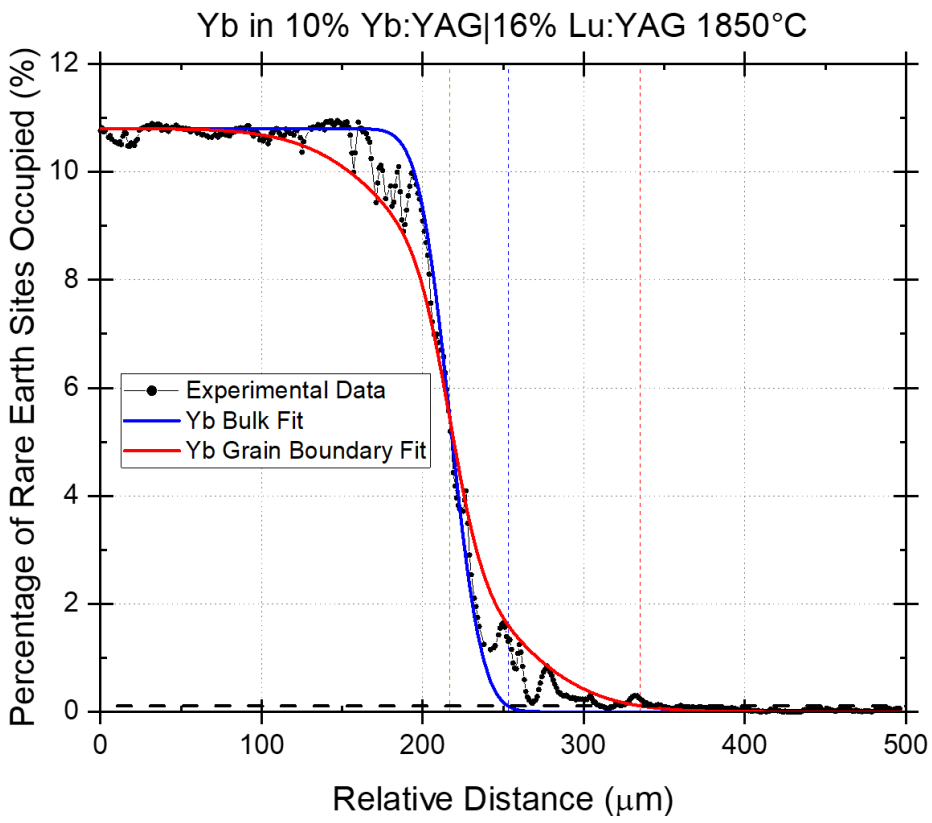

Figure 6. Experimental data with bulk and grain boundary fitting curves for Yb in 10%Yb:YAG|16% Lu:YAG processed at 1850°C. Fitting values are D=$3 \times 10^{-7}\ cm^2/_{hr}$ for the bulk curve and F=0.45, D_1=$3 \times 10^{-7}\ cm^2/_{hr}$, and D_2=$4 \times 10^{-6}\ cm^2/_{hr}$ for the grain boundary curve. Diffusion distance values, addressed later in this section, were derived from the distance between the composition interface to the location at which the concentration of the fit curve is equal to 1% of the maximum concentration.

Examples of the fits deduced for all RE species in each sample appear in Figure 7. The curve fits for the Y, Lu and Nd RE ions in a 16% Lu:YAG|3% Nd:YAG sample are displayed in Figure 7(b). In cases of extensive grain boundary diffusion such as this, the grain boundary curves did not intersect the bulk curves at either end of the line scan due to the long diffusion lengths as is apparent in the electron micrograph in Figure 7(d). In contrast, for other 1850°C fits such as in Figure 7(a) and (c) for the case of 10% Yb:YAG|16% Lu:YAG (as reported in Figure 6 for only Yb), the curves took similar forms but did indeed intersect the limiting bulk curve values at both ends, as would have been the case if it extended sufficiently far from the compositional interface for 16% Lu:YAG|3% Nd:YAG as well. The most important point revealed in Figure 7 is that Lu diffuses much further in the presence of the Nd counter-ion relative to that of Yb, see the red curves and the micrographs in the lower panes.

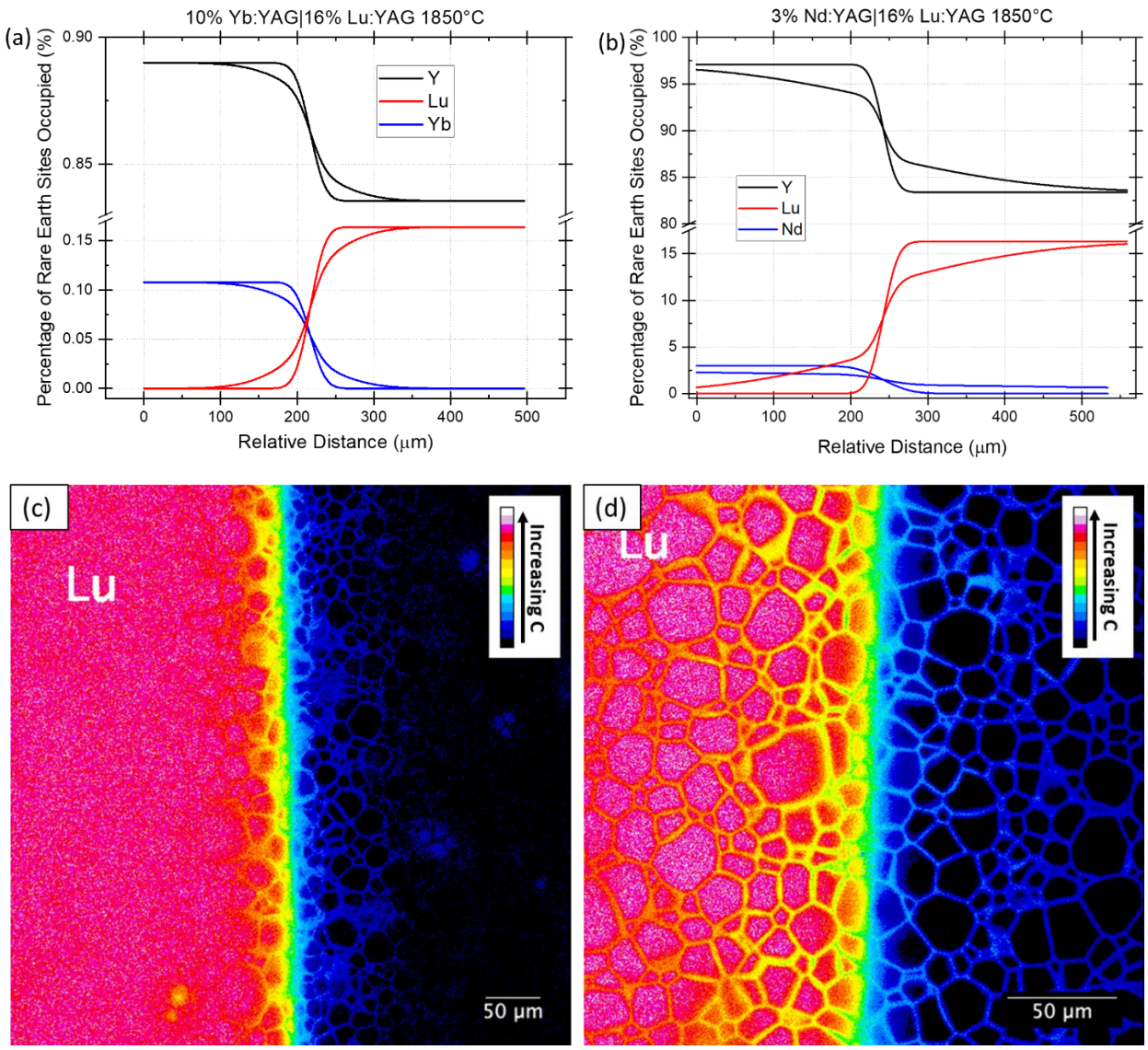

Figure 7. The curve fits (a) for all RE ions in a 10% Yb:YAG|16% Lu:YAG sample and (b) those in a 16% Lu:YAG|3% Nd:YAG sample. For all ions, the curve with the more gradual slope is that of the grain boundaries. Although the bulk and grain boundary fits do not converge for the dopants in (b), they did in most cases such as in (a) so it is presumed that (b) would show the same behavior if the data extended further from the composition boundary. As per Equation 2, the bulk curve concentrations, added together, sum to unity, as do the added grain boundary curves. Lu concentration maps for (a) and (b) are provided in (c) and (d), respectively, to reveal the dramatic difference in diffusion behavior of the same ion while a different dopant is counter diffusing.

Trends may be revealed by analyzing the diffusion constants shown in Table 1. For further clarity, diffusion distances from the composition interface, as designated based on the location at which the percentage of RE sites occupied equaled 1% of the maximum concentration [6] as noted in Figure 6, were plotted from the data in Table 1. For all samples, diffusion time during the HIP cycle was 4 hours (t = 4 hr in Equation 1). The resulting plots are given in Figure 8 and Figure 9. (Note that the 16% Lu:YAG|YAG sample processed at 1850°C is omitted in Table 1 due to an experimental mishap.)

Table 1. Diffusion constants and fractions for all samples, in cm^2/hr, for bulk and grain boundary (Gb) diffusion.

		Measured Dopant		
	1750 Bulk	Yb	Lu	Nd
Counter Dopant	None	1.00E-07	7.00E-08	5.00E-07
	Yb		7.00E-08	3.10E-07
	Lu	7.00E-08		2.70E-07
	Nd	5.00E-08	5.00E-08	

		Measured Dopant		
	1850 Bulk	Yb	Lu	Nd
Counter Dopant	None	2.00E-07		7.00E-07
	Yb		3.00E-07	1.00E-06
	Lu	3.00E-07		1.00E-06
	Nd	1.20E-07	3.00E-07	

		Measured Dopant		
	1750 Gb	Yb	Lu	Nd
Counter Dopant	None	2.20E-07	1.34E-06	2.00E-06
	Yb		2.20E-07	1.83E-06
	Lu	3.40E-07		1.50E-06
	Nd	2.50E-07	3.00E-07	

		Measured Dopant		
	1850 Gb	Yb	Lu	Nd
Counter Dopant	None	4.00E-06		4.00E-04
	Yb		4.00E-06	7.00E-04
	Lu	4.00E-06		6.00E-04
	Nd	7.00E-05	3.50E-05	

		Measured Dopant		
	1750 Bulk Fraction (F)	Yb	Lu	Nd
Counter Dopant	None	0.70	0.80	0.80
	Yb		0.70	0.70
	Lu	0.70		0.50
	Nd	0.70	0.50	

		Measured Dopant		
	1850 Gb Bulk fraction (F)	Yb	Lu	Nd
Counter Dopant	None	0.45		0.40
	Yb		0.45	0.45
	Lu	0.45		0.35
	Nd	0.60	0.45	

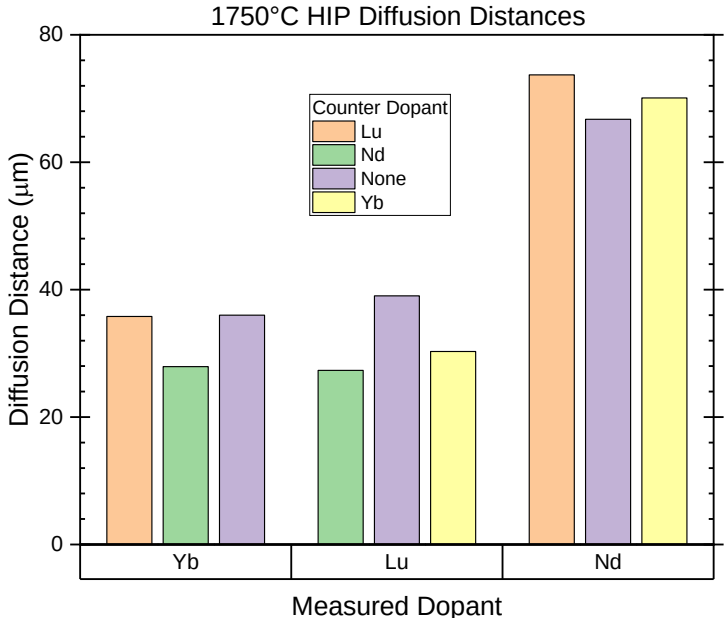

Figure 8. Diffusion distances measured for each dopant/counter dopant combination in the 1750°C samples. Diffusion time is 4 hours.

One trend in the 1750°C sample data (Figure 8) is that the presence of Nd as a counter dopant inhibited the diffusion of both Yb and Lu. Nd ions (112 pm for 8-fold coordination) are large relative to those of Yb (102 pm), Lu (97 pm), and Y (102 pm) and thus they distort the YAG structure to a higher

degree when they replace Y substitutionally. As a result, it appears to be more difficult for the other ions to diffuse when the lattice is under more strain. Another trend is that Nd diffused further than either of the other dopants, regardless of the counter ion species. This holds true in the 1850°C data as well (Figure 9), for both the bulk and grain boundary components. Note again that data for a 16% Lu:YAG|YAG sample processed at 1850°C is omitted due to loss of the sample before measurement.

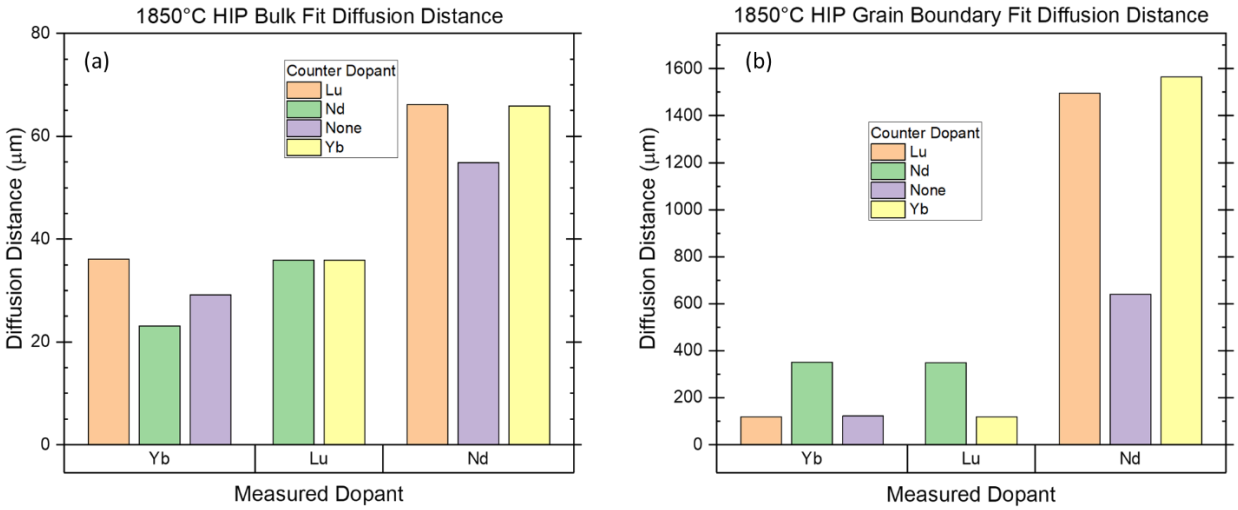

Figure 9. Diffusion distances, separated into (a) bulk and (b) grain boundary components, measured for each dopant/counter dopant combination in the 1850°C samples. Note the large difference in scale for the y axis.

In the case of the grain boundary diffusion at 1850°C, the counter-ion effect is even more pronounced, with Nd diffusion reaching distances from the interface in excess of 1.4 mm when a counter ion was present. Although the Nd ions have a driving force to segregate to the grain boundaries due to their size relative to the host lattice, corresponding to a segregation coefficient far less than 1 (k~0.2) as has been reported in other work [23], this does not necessarily explain why it diffused further when at the boundaries. However, it seems plausible that this driving force is indirectly responsible, in that the diminished capability of Nd to enter grains from the boundaries induces the Nd ions to travel further along the boundaries to alleviate the concentration gradient.

Another consistent trend throughout all data sets was that Nd always diffused further when a counter dopant was present than when undoped YAG was the other material forming the composition interface. This trend may result from an energetic penalty for removing Y from the lattice into the boundaries which would be present because a regular position in a crystal lattice will be a lower energy state than a position in the pseudo-amorphous boundaries. An increased concentration of Y at the boundaries is necessary so it can move in the direction opposite to the Nd to maintain charge neutrality. It should be somewhat easier for dopant ions to make the transition from a grain into the boundary because some degree of local strain on the lattice, present due to differences in ionic radii relative to Y, will reduce the energy penalty because it is starting in a higher-energy state than a Y ion in an unstrained lattice.

It can be observed in the 1850°C grain boundary data (Figure 9(b)) that, unlike the 1750°C data and the 1850°C bulk data, the presence of Nd increased the diffusion distance of the other dopants. This can be attributed to the required maintenance of charge neutrality; the long-distance migration of Nd ions necessitates an equally long migration of other positively charged species in the opposite direction and thus forces the other ions to diffuse faster than they would otherwise. Although it cannot be seen in the 1750°C data, it is expected that the same process occurs in those samples, but the inability to separate the bulk and grain boundary responses in these data, coupled with contribution fractions (F) favoring the bulk component (F>0.5) (Table 1) may just be dominant enough to hide the trend.

4. Conclusions

Compositional analysis of bilayer samples, where each layer was either undoped YAG or YAG doped with Yb, Lu, or Nd, were conducted after fabrication at both 1750°C and 1850°C to determine diffusion behavior of each dopant in the presence of the others. We found that the complementary error function equation with one diffusion coefficient was insufficient to fully fit the experimental concentration profiles. This was a direct result of both grain boundary and bulk diffusion simultaneously playing a role in dopant migration. It was verified that the ionic size of the dopant (segregation coefficient) affects relative dopant concentration at the grain boundaries, which propagates into affecting total migration distance. The presence of a counter dopant moving in the opposite direction can either enhance or inhibit diffusion of the primary dopant, depending on the respective segregation coefficients. Specifically, it was found that the large Nd counter ion tends to slow down bulk diffusion of Yb and Lu, while at the same time speeding up grain-boundary diffusion. Nd itself diffused further than either of the other dopants, regardless of the counter ion species or the processing temperature and diffused even further when a counter dopant was present than when undoped YAG was the other material forming the composition interface. All the observed trends were attributed to a combination of intragranular lattice strain due to dopant ions replacing yttrium substitutionally, the relative driving forces for the segregation of dopant ions to grain boundaries, and the ability of one dopant to affect the diffusion of a different dopant in the other direction to maintain charge neutrality. The results presented herein should assist in the design of additively manufactured laser gain media featuring small scale regions with different dopants in contact with each other upon deposition by facilitating prediction of dopant migration during high temperature fabrication of the part and, in doing so, giving a better idea of the true resolution limit of such features in the final product.

Acknowledgements

This work was sponsored by LLNL LDRD 19-ER-006 and was performed under the auspices of the U. S. Department of Energy by Lawrence Livermore National Laboratory under contract DE-AC52-07NA27344. LLNL-JRNL-828696.

References

1. Li J, Pan Y, Zeng Y, Liu W, Jiang B, Guo J. The history, development, and future prospects for laser ceramics: a review. International Journal of Refractory Metals and Hard Materials. 2013 Jul 1;39:44-52.

2. Yang H, Zhang J, Luo D, Lin H, Shen D, Tang D. Novel transparent ceramics for solid-state lasers. High Power Laser Science and Engineering. 2013 Dec;1(3-4):138-47.
3. Basiev TT, Doroshenko ME, Konyushkin VA, Osiko VV, Fedorov PP, Demidenko VA, Dukel'skii KV, Mironov IA, Smirnov AN. Fluoride optical nanoceramics. Russian Chemical Bulletin. 2008 May;57(5):877-86.
4. Jones IK, Seeley ZM, Cherepy NJ, Duoss EB, Payne SA. Direct ink write fabrication of transparent ceramic gain media. Optical Materials. 2018 Jan 1;75:19-25.
5. Hollingsworth JP, Kuntz JD, Soules TF. Neodymium ion diffusion during sintering of Nd: YAG transparent ceramics. Journal of Physics D: Applied Physics. 2009 Feb 5;42(5):052001.
6. Fujioka K, Sugiyama A, Fujimoto Y, Kawanaka J, Miyanaga N. Ion diffusion at the bonding interface of undoped YAG/Yb: YAG composite ceramics. Optical Materials. 2015 Aug 1;46:542-7.
7. Ma C, Tang F, Zhu J, Wen Z, Yu Y, Wang K, Du M, Zhang J, Long J, Yuan X, Guo W. Cation diffusion at the interface of composite YAG/Re: LuAG (Re= Nd or Yb) transparent ceramics. Journal of the European Ceramic Society. 2016 Aug 1;36(10):2555-64.
8. Seeley ZM, Phillips IR, Rudzik TJ, Cherepy NJ, Drobshoff AD, Payne SA. Material jet printing of transparent ceramic Yb: YAG planar waveguides. Optics Letters. 2021 May 15;46(10):2433-6.
9. Seeley ZM, Rudzik TJ, Phillips IR, Yee TD, Cherepy NJ, Drobshoff AD, Herrera OD, Ryerson FJ, Payne SA. Additive Manufacturing of Transparent Ceramic Laser Gain Media-Rods, Thin Disks, and Planar Waveguides. In Advanced Solid State Lasers 2020 Oct 13 (pp. AW1A-1). Optical Society of America.
10. Seeley ZM, Cherepy N, Rudzik T, Phillips I, Drobshoff A, Yee T, Herrera O, Ryerson F, Wineger T, Wang Y, Squillante M. 3D printed ceramic laser gain media. In Laser Technology for Defense and Security XVI 2021 Apr 19 (Vol. 11724, p. 117240B). International Society for Optics and Photonics.
11. Jones IK, Seeley Z, Cherepy N, Zhu C, Duoss E, Payne S. Functionally Graded Solid-State Laser Gain Media Fabricated by Direct Ink Write and Ceramic Processing. In Advanced Solid State Lasers 2016 Oct 30 (pp. AW3A-2). Optical Society of America.
12. Hasegawa K, Ichikawa T, Takeda Y, Ikesue A, Ito H, Motohiro T. Lasing characteristics of refractive-index-matched composite Y3Al5O12 rods employing transparent ceramics for solar-pumped lasers. Japanese Journal of Applied Physics. 2018 Mar 22;57(4):042701.
13. Seeley Z, Yee T, Cherepy N, Drobshoff A, Herrera O, Ryerson R, Payne SA. 3D printed transparent ceramic YAG laser rods: Matching the core-clad refractive index. Optical Materials. 2020 Sep 1;107:110121.
14. Ge L, Li J, Zhou Z, Qu H, Dong M, Zhu Y, Xie T, Li W, Chen M, Kou H, Shi Y. Fabrication of composite YAG/Nd: YAG/YAG transparent ceramics for planar waveguide laser. Optical Materials Express. 2014 May 1;4(5):1042-9.
15. Seeley ZM, Rudzik TJ, Phillips IR, Yee TD, Cherepy NJ, Drobshoff AD, Herrera OD, Ryerson FJ, Payne SA. Additive Manufacturing of Transparent Ceramic Laser Gain Media-Rods, Thin Disks, and Planar Waveguides. In Advanced Solid State Lasers 2020 Oct 13 (pp. AW1A-1). Optical Society of America.
16. Calignano F, Manfredi D, Ambrosio EP, Biamino S, Lombardi M, Atzeni E, Salmi A, Minetola P, Iuliano L, Fino P. Overview on additive manufacturing technologies. Proceedings of the IEEE. 2017 Jan 2;105(4):593-612.
17. Smigelskas AD. Zinc diffusion in alpha brass. Trans. Aime. 1947;171:130-42.
18. Donovan, JJ, Singer, JW, and Armstrong, JT, A new EPMA method for fast trace element analysis in simple matrices, American Mineralogist, 101, 1839-1853, doi: 10.2138/am-2016-5628 (2016)
19. Armstrong, JT, CITZAF - a package of correction programs for the quantitative electron microbeam x-ray-analysis of thick polished materials, thin-films, and particles, Microbeam Analysis, 4, 177-200 (1995)
20. OriginPro 2020 (Version 9.7) [Computer Software] OriginLab Corporation, Northampton, MA, https://www.OriginLab.com

21. Boulesteix R, Maitre A, Baumard JF, Rabinovitch Y, Sallé C, Weber S, Kilo M. The effect of silica doping on neodymium diffusion in yttrium aluminum garnet ceramics: implications for sintering mechanisms. Journal of the European Ceramic Society. 2009 Sep 1;29(12):2517-26.
22. Harrison LG. Influence of dislocations on diffusion kinetics in solids with particular reference to the alkali halides. Transactions of the Faraday Society. 1961;57:1191-9.
23. Chani VI, Boulon G, Zhao W, Yanagida T, Yoshikawa A. Correlation between segregation of rare earth dopants in melt crystal growth and ceramic processing for optical applications. Japanese Journal of Applied Physics. 2010 Jul 20;49(7R):075601.